

Relationship between the boson peak and first sharp diffraction peak in glasses

Running title: Boson peak dynamics in glass

Dan Kyotani^{1,†}, Soo Han Oh^{1,†}, Suguru Kitani², Yasuhiro Fujii^{3,4}, Hiroyuki Hijiya⁵, Hideyuki Mizuno⁶, Shinji Kohara⁷, Akitoshi Koreeda⁸, Atsunobu Masuno⁹, Hitoshi Kawaji², Seiji Kojima¹, Yohei Yamamoto¹, Tatsuya Mori^{1*}

¹Department of Materials Science, University of Tsukuba, 1-1-1 Tennodai, Tsukuba, Ibaraki 305-8573, Japan

²Materials and Structures Laboratory, Institute of Integrated Research, Institute of Science Tokyo, 4259 Nagatsuta, Midori-ku, Yokohama 226-8501, Japan

³Institute for Open and Transdisciplinary Research Initiatives, Osaka University, 2-1 Yamadaoka, Suita, Osaka 565-0871, Japan

⁴Research Organization of Science and Technology, Ritsumeikan University, 1-1-1 Noji-higashi, Kusatsu, Shiga 525-8577, Japan

⁵Materials Integration Laboratories, AGC Inc., 1-1 Suehiro-cho, Tsurumi-ku, Yokohama 230-0045, Japan

⁶Graduate School of Arts and Sciences, The University of Tokyo, 3-8-1 Komaba, Meguro-ku, Tokyo 153-8902, Japan

⁷Center for Materials Research by Information Integration (CMI2), Research and Services Division of Materials Data and Integrated System (MaDIS), National Institute for Materials Science (NIMS), 1-1 Namiki, Tsukuba, Ibaraki 305-0044, Japan

⁸Department of Physical Sciences, Ritsumeikan University, 1-1-1 Noji-higashi, Kusatsu, Shiga 525-8577, Japan

⁹Graduate School of Engineering, Kyoto University, Kyotodaigaku-Katsura, Nishikyo-ku, Kyoto 615-8520, Japan

*Corresponding author

Email: mori@ims.tsukuba.ac.jp (T. Mori)

†These authors contributed equally to this work.

Abstract

Boson peak (BP) dynamics refers to the universal excitation in the terahertz region of glass. In this study, the universal dynamics of BP were quantitatively evaluated in various glassy materials

based on the heterogeneous elasticity theory (HET), and the determinants of BP were successfully extracted. A strong correlation was observed between the maximum possible coarse-graining wavenumber, which is a determinant of the BP in the HET, and the first sharp diffraction peak (FSDP) wavenumber, which is a characteristic index of the medium-range order in glasses. The results indicate that the behaviour of BP in glass can be quantitatively understood in the following two steps. First, the FSDP representing the largest structural correlation in glass is dominantly used to determine the unit size of the elastic modulus heterogeneity, and second, the magnitude of the elastic modulus fluctuation is used to determine the frequency and intensity of the BP.

Introduction

A universal excitation called the boson peak (BP) is observed in glass-forming materials in the terahertz (THz) region, which is the frequency band at the end of sound waves^{1,2}. The BP is observed as the excess vibrational density of states (v-DOS, $g(\omega)$) deviating from the Debye model that describes crystal sound waves. Because the v-DOS of the Debye model is proportional to ω^{D-1} for D -dimensional materials, where ω is the angular frequency, the BP appears as a peak in the $g(\omega)/\omega^{D-1}$ spectrum.

BP is the origin or trigger of various phenomena related to glassy materials, such as their ultralow thermal conductivity compared to crystals³, microscopic plastic deformation of glass⁴ and the beginning of THz band optical absorption in glass^{5,6}. Thus, BP excitation significantly contributes to the thermal, mechanical, and optical properties of glass, and the understanding of its mechanism and its applications are expected to be paramount. However, despite numerous experiments^{3,5-13} including computer simulations^{4,14-19}, and theoretical proposals²⁰⁻²⁵ on the origin of BP over the last few decades, no consensus has been reached.

As a BP theory, heterogeneous elasticity theory (HET) is well known and allows for a quantitative interpretation of BP behaviour^{20,26-28}. The HET model incorporates spatial fluctuations into the shear modulus in the equation of motion of an isotropic elastic body, i.e. the ‘Navier equation’, considering the structural disorder of glass. The basic equations are as follows:

$$\frac{\partial^2 \mathbf{u}(\mathbf{r}, t)}{\partial t^2} = \frac{1}{\rho} \nabla \cdot \left(\left(K + \frac{4}{3} G(\mathbf{r}) \right) \nabla \cdot \mathbf{u}(\mathbf{r}, t) \right) - \frac{1}{\rho} \nabla \times (G(\mathbf{r}) \nabla \times \mathbf{u}(\mathbf{r}, t)), \quad (1)$$

where $\mathbf{u}(\mathbf{r}, t)$ is the positional \mathbf{r} and time t dependent displacement in the continuum. K and $G(\mathbf{r})$ are the bulk modulus and the shear modulus with spatial fluctuations, respectively, and ρ is the mass density. In Navier or simple wave equations, the elastic moduli (K and G) and density ρ are treated as constants. This is equivalent to treating a homogeneous continuum or crystal. However, the HET model incorporates spatial heterogeneity in G owing to the structural disorder of the glassy system.

A technique used to solve Eq. (1) is the coherent potential approximation (CPA), which is a

mean-field approximation^{26,28,29}. This approximation makes it possible to replace the spatially heterogeneous shear modulus ($G(\mathbf{r})$ in Eq. (1) or \tilde{G}_i in Eq. (2) (see Methods)) with a spatially uniform frequency-dependent complex shear modulus $G(\omega)$. The CPA model can treat large heterogeneities in the elastic modulus and can therefore reproduce the large BP intensity of some glasses (e.g. silica glass), which could not be reproduced in previously reported HET models (see Figure 1 of ref. 8). In the CPA model^{26,28}, two main determinants of BP are present: 1) the magnitude of the elastic modulus fluctuations, and 2) the length of the spatial correlation of the elastic heterogeneity. However, understanding how these factors are related to the actual physical properties of glass remains open.

Furthermore, connecting the parameters of the model with real physical properties is required for the HET to explain the BP of real materials. In particular, the relationship between the elastic heterogeneity and the microscopic glass structure, especially the medium-range order of the glass, is not understood. The first sharp diffraction peak (FSDP) is a representative indicator of medium-range order. The FSDP appears as a strong peak at the lowest angle in the structure factor $S(k)$ of the glass^{30,31}, where k is the wavenumber. The reciprocal of FSDP indicates the size of the pseudo-lattice of the glass, corresponding to the size of the unit cell in the case of a crystal. Although the relationship between the FSDP and BP has been discussed for various glasses^{32–35}, a universal relationship is yet to be demonstrated. Therefore, even in the HET framework, the relationship between the descriptors of the theory and the medium-range order has not been established. This obscures the picture of HET in actual glass, and in some cases, causes HET to be rejected^{36,37}.

In this study, we first performed CPA analysis based on HET on typical glasses, i.e. inorganic silica glass (SiO_2) and organic glycerol glass, to extract the nanomechanical properties that can reproduce the BP of glasses. Subsequently, we performed CPA on various glasses to investigate the relationship between the medium-range order of glasses and the spatial correlation length of elastic heterogeneity, which is a determinant of BP in the CPA model. We found that the spatial correlation of the elastic modulus was dominated by the pseudo-lattice size, which is determined by the FSDP of the glass. Finally, we concluded that the two properties of BP—frequency and intensity—can be explained by two factors, namely the pseudo-lattice size of the glass and the elastic heterogeneity magnitude.

Methods

Coherent potential approximation (CPA) analysis

To obtain the normalised effective shear modulus $\tilde{G}(z)$ ($z = \omega + i\epsilon$), the following CPA equation was solved numerically²⁸:

$$\left\langle \frac{\tilde{G}_i - \tilde{G}(z)}{1 + \frac{1}{3}[\tilde{G}_i - \tilde{G}(z)]\Lambda(k_e, z)} \right\rangle_P = 0, \quad (2)$$

where \tilde{G}_i is the mass-density-normalised shear modulus with spatial fluctuations defined by $\tilde{G}_i = G_i/\rho \equiv G(\mathbf{r}_i)/\rho$. $\tilde{G}(z)$ is the mass-density-normalised effective shear modulus, defined as $\tilde{G}(z) = G(z)/\rho$. In Eq. (2), to reproduce the BP frequency and intensity of various glasses, we used the following log-normal distribution function:

$$P(\tilde{G}_i, \tilde{G}_0, \sigma) = \frac{1}{\sigma\sqrt{2\pi}} \frac{1}{\tilde{G}_i} \exp\left\{-\frac{1}{2\sigma^2} [\ln(\tilde{G}_i/\tilde{G}_0)]^2\right\}, \quad (3)$$

where $\tilde{G}_0 = G_0/\rho$ is the mass-density-normalised geometric mean of G_i . σ^2 is the disorder parameter of spatial distribution of shear modulus, which is related to variance $\text{Var}[\tilde{G}_i]$ by $\sigma^2 = \ln\{1 + \text{Var}[\tilde{G}_i]/\langle\tilde{G}_i\rangle^2\}$ ²⁸. Although we recognise that the distribution of elastic heterogeneity in real glasses does not generally follow a log-normal distribution, we chose the log-normal distribution function to investigate the properties of BP (BP frequency and intensity) with two unified parameters (k_e and σ^2) in the CPA. Notably, for small σ^2 , the line shapes of the log-normal distribution and the Gaussian distribution show similar behaviour, as depicted in Supplementary Figure S1 and these distributions constitute a similar BP spectrum shape.

The integral kernel $\Lambda(k_e, z)$ in Eq. (2) is as follows:

$$\Lambda(k_e, z) = \frac{3}{k_e^3} \int_0^{k_e} dk k^4 \left(\frac{4}{3} \mathcal{G}_L(k, z) + 2\mathcal{G}_T(k, z) \right), \quad (4)$$

where k_e is the maximum possible coarse-grained wavenumber. The reciprocal of k_e , i.e. the minimum possible coarse-graining length λ_e has a physical interpretation as the correlation length of spatial fluctuations of the shear modulus^{38,39}. The relationship between k_e and λ_e is as follows²⁸:

$$k_e = \sqrt[3]{2\pi^2/\lambda_e}. \quad (5)$$

Green's functions for the longitudinal wave $\mathcal{G}_L(k, \omega)$ and transverse wave $\mathcal{G}_T(k, \omega)$ are defined as follows:

$$\mathcal{G}_L(k, z) = \frac{1}{-z^2 + k^2 v_L(z)^2}, \quad (6a)$$

$$\mathcal{G}_T(k, z) = \frac{1}{-z^2 + k^2 v_T(z)^2}, \quad (6b)$$

where the complex frequency-dependent transverse sound velocity $v_T(z)$ and complex frequency-dependent longitudinal sound velocity $v_L(z)$ are related to $\tilde{G}(z)$ and the experimental bulk modulus K_{exp} by the following relationships:

$$v_T(z)^2 = \tilde{G}(z), \quad (7a)$$

$$v_L(z)^2 = \frac{K_{\text{exp}}}{\rho} + \frac{4}{3}\tilde{G}(z). \quad (7b)$$

The input parameters for solving Eq. (2) show the experimental data of transverse v_T and longitudinal v_L sound velocities. When $z = 0$ and $v_T^2 = \tilde{G}(0)$, the relationship between $\tilde{G}(0)/\tilde{G}_0$ and σ as an implicit function is detailed in the Appendix of Ref. 28.

The vibrational density of states $g(\omega)$ is expressed as follows:

$$g(\omega) = \text{Im} \left[\frac{2\omega}{3\pi} \frac{3}{k_D^3} \int_0^{k_D} dk k^2 (\mathcal{G}_L(k, \omega) + 2\mathcal{G}_T(k, \omega)) \right], \quad (8)$$

where the Debye wavenumber k_D is defined as $k_D = \sqrt[3]{6\pi^2 N/V}$. N and V are the number of particles and the volume of the system, respectively.

The fits for SiO₂ and glycerol were performed using the least squares method (Figure S1). For other glasses, k_e and σ were determined to reproduce the BP frequency and intensity (see Table S1).

Results

As shown in the BP spectra $g(\omega)/\omega^2$ in Figure 1(a), the BP frequencies of typical inorganic SiO₂ and typical organic glycerol glass are both located at approximately 1 THz, and their BP heights are almost the same^{40,41}. However, the Debye levels of the two materials are significantly different, and the Debye level of SiO₂ is low because of its large sound velocity. This indicates that the BP intensity of SiO₂ is much higher than that of glycerol. This difference is clarified in the normalised BP spectrum shown in Figure 1(b). The horizontal and vertical axes were normalised using the Debye frequency $\omega_D = [18\pi^2(N/V)/(2v_T^{-3} + v_L^{-3})]^{1/3}$ and Debye level $A_D = 3/\omega_D^3$, respectively. N and V are the number of particles and volume of the system, respectively. Moreover, v_T and v_L are the transverse and longitudinal sound velocities, respectively. The normalised spectrum shows that SiO₂ has a lower BP frequency and a much higher BP intensity than glycerol.

To reproduce these spectra using HET and discuss the differences in the properties of BP using unified parameters, we fitted the experimental spectra with the CPA equation using the log-normal distribution function with the maximum possible coarse-graining wavenumber k_e and the disorder parameter σ^2 as independent parameters (see Methods). The G_0 , which is a geometric mean of $G(\mathbf{r})$, in the log-normal distribution function is implicitly related to σ ²⁸. The extracted parameters G_0 , k_e and σ are summarised in Table 1, and the obtained complex moduli $G(\omega)$ of SiO₂ and glycerol are shown in Supplementary Figure S1.

The $g(\omega)$ was calculated using Green's function, including $G(\omega)$ (see Eq. (8) in Methods), and the obtained $g(\omega)/\omega^2$ is shown in Figure 1(b) using solid lines. The BP frequency and intensity of the calculated spectra were both in good agreement with the experimental results.

Regarding the line shapes of CPA, although the line shape of glycerol agrees well with the experimental spectrum, the result of SiO₂ considerably deviates from the experimental result. Modifications are required in the CPA to correct this deviation, such as applying a probability density function that reproduces the v-DOS of silicate glasses; however, this is beyond the scope of this study.

To understand the origin of the different BP behaviours of SiO₂ and glycerol, we discuss the $k_e - \sigma^2$ dependence of the normalised BP frequency and intensity, as shown in Figure 2. The normalised k_e values of the two substances were found to be almost the same; however, in contrast, σ^2 of SiO₂ is 2.3 times larger than that of glycerol. The normalised BP frequency and intensity obtained by solving the CPA equation with $v_L/v_T = 2$, which is a typical ratio for various glasses, as input parameters are shown in the colour map. This colour map shows that when k_e is fixed and σ^2 increases, the BP frequency decreases (Figure 2(a)), whereas the BP intensity increases (Figure 2(b)). Thus, comparing the two materials, a large σ^2 of SiO₂ decreases the BP frequency and increases the BP intensity compared with glycerol.

Furthermore, we visualised the obtained parameters k_e and σ using the glass structure (see SI) in real space and discussed their physical meaning. First, in Figure 3, the reciprocal of the maximum possible coarse-graining wavenumber k_e , i.e. the minimum possible coarse-graining wavelength λ_e defined by Eq. (5), is displayed on an actual scale as the lattice size of the grid lines. The lattice sizes indicate λ_e of each material, which is ~ 3 Å for both materials. In addition, the dimensions of the glass structures in Figure 3 indicate wavelengths of $\lambda_{\text{BP-SiO}_2} = 38.0$ Å and $\lambda_{\text{BP-Gly}} = 19.6$ Å of the BP modes of SiO₂ and glycerol, respectively. Here, the wavelength of the BP mode λ_{BP} is the same as what is generally called the characteristic length of BP. The wavelength is defined by $\lambda_{\text{BP}} = 2\pi v_T/\omega_{\text{BP}}$.

Moreover, we found that the λ_{BP} values of SiO₂ and glycerol were considerably different, and the ratio of λ_{BP} to λ_e was as large as 12 for SiO₂ and 6 for glycerol. This difference in the $\lambda_{\text{BP}}/\lambda_e$ ratio is due to the difference in the magnitude of the fluctuation of the shear modulus of the two materials, i.e. the difference in the magnitude of the disorder parameter σ^2 . This is shown in the glass structures depicted in Supplementary Figure S3 as colour distributions based on the log-normal distribution function obtained from the CPA analysis of each material. The greater the magnitude of the fluctuations in the shear modulus, the longer the wavelength and lower the normalised frequency of the BP mode, in which a rapid increase in the imaginary part of $G(\omega)$ starts toward the higher frequency in the effective medium (Supplementary Figures S2(a) and S2(c)). Consequently, a large σ^2 increases $\lambda_{\text{BP}}/\lambda_e$, i.e. it decreases the normalised BP frequency.

Next, we considered the physical meanings and origins of k_e and its reciprocal λ_e . Previous research⁴³ has shown that when shear modulus fluctuations have a spatial correlation, the

reciprocal of k_e approximately represents the length of the spatial correlation of the shear modulus. Considering this, the FSDP in the $S(k)$, which is an indicator of the medium-range order of glasses, is a natural candidate for the origin of the minimum length of the spatial correlation of the elastic modulus in glasses. Supplementary Figure S4 shows the structural factors $S(k)$ of SiO₂ and glycerol. As summarised in Table 1, the FSDP wavenumbers k_{FSDP} (or reciprocal $\lambda_{\text{FSDP}} = 2\pi/k_{\text{FSDP}}$) of SiO₂ and glycerol appear to agree well with their respective k_e (or λ_e).

The generality of this relationship was verified by performing CPA on various glasses and examining the correlation between k_e and k_{FSDP} . As shown in Figure 4, a strong positive correlation was observed between k_{FSDP} and k_e in various organic-to-inorganic glasses. Furthermore, the values of k_e and k_{FSDP} are of the same order. Note that we do not claim all glasses fall exactly on the fitting curve but emphasise that the fitting curve is indicative of the overall trend. These results lead to the following conjecture: ‘The minimum possible coarse-graining size of the elastic modulus of glass is dominantly determined by FSDP: The BP is caused by the inhomogeneous elasticity fluctuating for each size of the pseudo-lattice formed by FSDP’.

The relationship between the medium-range order in glasses and BP has been discussed^{32–35}. However, the correlation between k_{FSDP} and $k_{\text{BP}} = \omega_{\text{BP}}/v_{\text{T}}$ is not simple. Moreover, they appear to be uncorrelated, as shown in Supplementary Figure S5. However, based on our hypothesis, the relationship between k_{FSDP} and k_{BP} can be described in the following two steps. First, the minimum possible coarse-graining length λ_e of the elastic modulus is dominantly determined by λ_{FSDP} . As explained by the HET framework and shown in Figure 5, the ratio k_{BP}/k_e decreases as the disorder parameter σ^2 increases. In other words, as mentioned above, by increasing σ^2 , $\lambda_{\text{BP}}/\lambda_e$ increases or the normalised BP frequency decreases. In previous studies^{32–35}, the parameters k_e and σ^2 could not be separated; however, we clarified the quantitative relationship between k_e , a determinant of BP in the CPA, and the FSDP.

Furthermore, the scenario obtained in this study is applicable to the BP behaviour of simple glass with a Lennard–Jones (LJ) potential obtained by molecular dynamics (MD) simulations. We analysed the LJ glass⁴⁴ using the CPA equation, and the result is plotted by an open circle in Figure 4. In the $S(k)$ of the LJ glass, only one peak is present, which indicates the correlation between the neighbouring two atoms of simple glass (see Supplementary Figure S4). Therefore, we regarded the k indicating the position of one peak as k_{FSDP} . The result of the LJ glass shown in Figure 4 deviated from the glasses with FSDP, and the ratio of k_{FSDP}/k_e is 1.81 with $k_e/k_{\text{D}} = 0.238$. Furthermore, $\lambda_{\text{BP}}/\lambda_e = 5.5$ (see Supplementary Figure S6 and Supplementary Table S1). A recent study of MD simulation for simple glasses by Hu and Tanaka^{36,37} suggested that the HET scenario does not hold because the spatial correlation size of the spring-constant heterogeneity in LJ glasses is mismatched with the wavelength of the string-like structure of the

BP mode. The resolution of the spring-constant heterogeneity in their results (the resolution of the yellow-coloured area in Figure 5 of Ref. 36) is approximately two atoms, and the wavelength of BP is approximately 15 atoms. However, our analysis shows it is exactly the ratio of $\lambda_{\text{BP}}/\lambda_e$ as shown in Supplementary Figure S6, and the results of simple glasses can be also explained by the HET scenario.

In addition to the LJ glass, we performed CPA analysis on a physical gel system in MD simulations⁴⁴. The physical gel system utilised the LJ potential, but its density is anomalously lower than that of typical LJ glass (see Supplementary Figure S7 and figure 1(d) of ref. 42). Regarding structure, the system has two peaks in $S(k)$ (see Supplementary Figure S4). The peak for the higher wavenumber represents the correlation between the neighbouring two atoms, also existing in LJ glass. The other peak for the lower wavenumber appears due to voids that are unique to physical gels as shown in Supplementary Figure S7. The results of CPA analysis for the physical gels assuming k_{FSDP} as the lower peak are shown in Figure 4 by open squares. The characteristics of the physical gel results are located below the fitting curve of FSDP glasses. Consequently, physical gels, FSDP glasses and LJ glasses are in different regions of the $k_e/k_D - k_{\text{FSDP}}/k_D$ dependence. This is presumably due to the different properties of the lowest peaks in $S(k)$ for the three types of amorphous materials. It may seem unusual that the characteristic length of the heterogeneity of the elastic modulus has a strong relationship with the structure factor, i.e., density fluctuations. However, as shown in the CPA equation (Eq. (2)), HET is fundamentally a theory that addresses the inhomogeneity of the velocity field. Furthermore, the transverse sound velocity fluctuation $v_{\text{T}}(\mathbf{r})$ is related to the shear modulus $G(\mathbf{r})$ and mass density $\rho(\mathbf{r})$ fluctuations by $v_{\text{T}}(\mathbf{r})^2 = G(\mathbf{r})/\rho(\mathbf{r})$, and the mass density heterogeneity is essentially included in the velocity fluctuations. In the case of physical gels, the BP intensity is quite small (see Fig. 9 of ref. 42) even though the heterogeneity of the elastic modulus is noticeably large due to the presence of voids. The low BP intensity of physical gel is likely attributed to the small fluctuations of the average velocity field, as the elastic modulus and mass density are proportionally lower in the areas where voids are present.

In this study, we could not identify the physical origin of σ . Qualitatively, however, the presence of voids in the glass or the lower coordination number would produce a small local shear modulus and increase σ .

Discussion

In this study, the determinants of BP in the CPA based on the HET were extracted by quantitatively reproducing the typical BP behaviour of glasses (BP frequency and intensity). Regarding the physical origin of the maximum possible coarse-graining wavenumber k_e , which is a determining factor of BP, we found that k_e and k_{FSDP} , which is a characteristic index of the

medium-range order of glasses, showed not only a strong positive correlation, but also comparable values. This result implies that the unit of modulus heterogeneity is dominated by FSDP or the lowest peak in $S(k)$, exhibiting a pseudo-lattice-like structural correlation in the glass. Furthermore, the BP frequency and intensity can be understood quantitatively based on the magnitude of the elastic modulus fluctuation for that unit.

Although a correlation between k_e and FSDP was observed, quantitative elucidation of the physical origin of σ , which is qualitatively attributed to local connectivity, is left for future work. When the correlation between these determinants of BP in the HET and its physical properties is fully understood, a quantitative understanding of the physical phenomena caused by BP and the application of BP may be realised.

Acknowledgements

We thank Zhiwen Pan, Lothar Wondraczek and Walter Schirmacher for their useful discussions. We would like to thank Shogo Bando for his assistance with the CPA analysis of LJ glass and for visualizing the results. This work was supported by JSPS KAKENHI Grant Nos. 23H01139 (to T.M.), 23H04495 (to H.M.) and 22K03543 (to H.M.); and JSPS Grant-in-Aid for Transformative-Research Areas (A) ‘Hyper-Ordered Structures Science’ Grant Nos. 20H05878 (to S. Kohara) and 20H05881 (to S. Kohara); and the AGC research collaboration (to T.M.); and GIC & NGF (to T.M.).

Author contributions

T.M. conceived this study and wrote the paper, with contributions and discussions from all authors. D.K. and S.H.O performed CPA analysis for VDOS data. S. Kitani. and H. K. performed maximum entropy method analysis for low-temperature specific heat data. S. Kohara. performed reverse Monte Carlo simulations to obtain the SiO₂ glass structure. T.M., H.M., H.H., Y.F., A.K., A.M., Y.Y., and S. Kojima evaluated the determinant factors of BP. All authors were involved in manuscript revisions.

Conflict of interest

The authors declare no competing interests.

Data availability

The data that support the findings of this study are available from the corresponding author upon reasonable request.

References

- [1] Nakayama, T. Boson peak and terahertz frequency dynamics of vitreous silica. *Rep. Prog. Phys.* **65**, 1195–1242 (2002).
- [2] Ramos, M. A. *Low-temperature thermal and vibrational properties of disordered solids* (World Scientific, London, 2022).
- [3] Zeller, R. C. & Pohl, R. O. Thermal conductivity and specific heat of noncrystalline solids. *Phys. Rev. B* **4**, 2029–2041 (1971).
- [4] Tanguy, A., Mantsi, B. & Tsamados, M. Vibrational modes as a predictor for plasticity in a model glass. *Europhys. Lett.* **90**, 16004 (2010).
- [5] Kabeya, M. *et al.* Boson peak dynamics of glassy glucose studied by integrated terahertz-band spectroscopy. *Phys. Rev. B* **94**, 224204 (2016).
- [6] Mori, T. *et al.* Detection of boson peak and fractal dynamics of disordered systems using terahertz spectroscopy. *Phys. Rev. E* **102**, 022502 (2020).
- [7] Buchenau, U. *et al.* Low-frequency modes in vitreous silica. *Phys. Rev. B* **34**, 5665–5673 (1986).
- [8] Rufflé, B., Parshin, D. A., Courtens, E. & Vacher, R. Boson peak and its relation to acoustic attenuation in glasses. *Phys. Rev. Lett.* **100**, 015501 (2008).
- [9] Baldi, G., Giordano, V. M., Monaco, G. & Ruta, B. Sound attenuation at terahertz frequencies and the boson peak of vitreous silica. *Phys. Rev. Lett.* **104**, 195501 (2010).
- [10] Chumakov, A. I. *et al.* Equivalence of the boson peak in glasses to the transverse acoustic van Hove singularity in crystals. *Phys. Rev. Lett.* **106**, 225501 (2011).
- [11] Phillips, W. A. *Amorphous solids: Low-temperature properties* (Springer, Berlin, 1981).
- [12] Malinovsky, V. K. & Sokolov, A. P. The nature of boson peak in Raman scattering in glasses. *Solid State Commun.* **57**, 757–761 (1986).
- [13] Kojima, S. Low-frequency Raman investigation of the liquid-glass transition in glycerol. *Phys. Rev. B* **47**, 2924–2927 (1993).
- [14] Franz, S., Parisi, G., Urbani, P. & Zamponi, F. Universal spectrum of normal modes in low-temperature glasses. *Proc. Natl. Acad. Sci.* **112**, 14539–14544 (2015).
- [15] Shintani, H. & Tanaka, H. Universal link between the boson peak and transverse phonons in glass. *Nat. Mater.* **7**, 870–877 (2008).
- [16] Lerner, E., Düring, G. & Bouchbinder, E. Statistics and properties of low-frequency vibrational modes in structural glasses. *Phys. Rev. Lett.* **117**, 035501 (2016).
- [17] Mizuno, H., Shiba, H. & Ikeda, A. Continuum limit of the vibrational properties of amorphous solids. *Proc. Natl. Acad. Sci. U.S.A.* **114**, E9767–E9774 (2017).

- [18] Tomoshige, N., Mizuno, H., Mori, T., Kim, K. & Matubayasi, N. Boson peak, elasticity, and glass transition temperature in polymer glasses: Effects of the rigidity of chain bending. *Sci. Rep.* **9**, 19514 (2019).
- [19] Tomoshige, N. *et al.* Understanding the scaling of boson peak through elastic heterogeneity insensitive to bending rigidity in polymer glasses. *J. Phys.: Condens. Matter* **33**, 274002 (2021).
- [20] Schirmacher, W. Thermal conductivity of glassy materials and the ‘boson peak’. *Europhys. Lett.* **73**, 892–898 (2006).
- [21] Schirmacher, W., Ruocco, G. & Scopigno, T. Acoustic attenuation in glasses and its relation with the boson peak. *Phys. Rev. Lett.* **98**, 025501 (2007).
- [22] Wyart, M. Scaling of phononic transport with connectivity in amorphous solids. *Europhys. Lett.* **89**, 64001 (2010).
- [23] Degiuli, E., Laversanne-Finot, A., Düring, G., Lerner, E. & Wyart, M. Effects of coordination and pressure on sound attenuation, boson peak and elasticity in amorphous solids. *Soft Matter* **10**, 5628–5644 (2014).
- [24] Buchenau, U., Galperin, Y. M., Gurevich, V. L. & Schober, H. R. Anharmonic potentials and vibrational localization in glasses. *Phys. Rev. B* **43**, 5039–5045 (1991).
- [25] Parshin, D. A., Schober, H. R. & Gurevich, V. L. Vibrational instability, two-level systems, and the boson peak in glasses. *Phys. Rev. B* **76**, 064206 (2007).
- [26] Köhler, S., Ruocco, G. & Schirmacher W. Coherent potential approximation for diffusion and wave propagation in topologically disordered systems. *Phys. Rev. B* **88**, 064203 (2013).
- [27] Schirmacher, W., Scopigno, T. & Ruocco, G. Theory of vibrational anomalies in glasses. *J. Non-Cryst. Solids* **407**, 133–140 (2015).
- [28] Pan, Z. *et al.* Disorder classification of the vibrational spectra of modern glasses. *Phys. Rev. B* **104**, 134106 (2021).
- [29] Yonezawa, F. & Morigaki, K. Coherent potential approximation. Basic concepts and applications. *Prog. Theor. Phys. Suppl.* **53**, 1–76 (1973).
- [30] Salmon, P. S. Real space manifestation of the first sharp diffraction peak in the structure factor of liquid and glassy materials. *Proc. R. Soc. Lond. A* **445**, 351–365 (1994).
- [31] Onodera, Y. *et al.* Structure and properties of densified silica glass: Characterizing the order within disorder. *NPG Asia Mater.* **12**, 85 (2020).
- [32] Sokolov, A. P., Kiskiuk, A., Soltwisch, M. & Quitmann, D. Medium-range order in glasses: Comparison of Raman and diffraction measurements. *Phys. Rev. Lett.* **69**, 1540–1543 (1992).
- [33] Elliott, S. R. A unified model for the low-energy vibrational behaviour of amorphous solids. *Europhys. Lett.* **19**, 201–206 (1992).
- [34] Uchino, T. & Yoko, T. Low-frequency Raman scattering and the fast relaxation process in glycerol. *Science* **273**, 480–483 (1996).

- [35] Inamura, Y. *et al.* Intermediate range structure and low-energy dynamics of densified vitreous silica. *J. Non-Cryst. Solids* **293–295**, 389–393 (2001).
- [36] Hu, Y.-C. & Tanaka, H. Origin of the boson peak in amorphous solids, *Nat. Phys.* **18**, 669–677 (2022).
- [37] Hu, Y.-C. & Tanaka, H. Universality of stringlet excitations as the origin of the boson peak of glasses with isotropic interactions, *Phys. Rev. Res.* **5**, 023055 (2023).
- [38] Schmid, B. & Schirmacher, W. Raman Scattering and the Low-Frequency Vibrational Spectrum of Glasses. *Phys. Rev. Lett.* **100**, 137402 (2008).
- [39] Schirmacher, W., Tomaras, C., Schmid, B., Baldi, G., Viliani, G., Ruocco, G. & Scopigno, T. Sound attenuation and anharmonic damping in solids with correlated disorder. *Condens. Matter Phys.* **13**, 23606 (2010).
- [40] Wischnewski, A., Buchenau, U., Dianoux, A. J., Kamitakahara, W. A. & Zarestky, J. L. Sound-wave scattering in silica. *Phys. Rev. B* **57**, 2663–2666 (1998).
- [41] Wuttke, J. *et al.* Fast dynamics of glass-forming glycerol. *Phys. Rev. E* **52**, 4026–4034 (1995).
- [42] Stukowski, A. Visualization and analysis of atomistic simulation data with OVITO—the open visualization tool. *Modeling Simul. Mater. Sci. Eng.* **18**, 015012 (2010).
- [43] Schirmacher, W. *et al.* Sound attenuation and anharmonic damping in solids with correlated disorder. *Condens. Matter Phys.* **13**, 23606 (2010).
- [44] Mizuno, H., Hachiya M. & Ikeda, A. Structural, mechanical, and vibrational properties of particulate physical gels. *J. Chem. Phys.* **155**, 234502 (2021).
- [45] Champeney, D. C., Joarder, R. N. & Dore, J. C. Structural studies of liquid D-glycerol by neutron diffraction. *Mol. Phys.* **58**, 337–347 (1986).
- [46] Scarponi, F., Comez, L., Fioretto, D. & Palmieri, L. Brillouin light scattering from transverse and longitudinal acoustic waves in glycerol. *Phys. Rev. B* **70**, 054203 (2004).

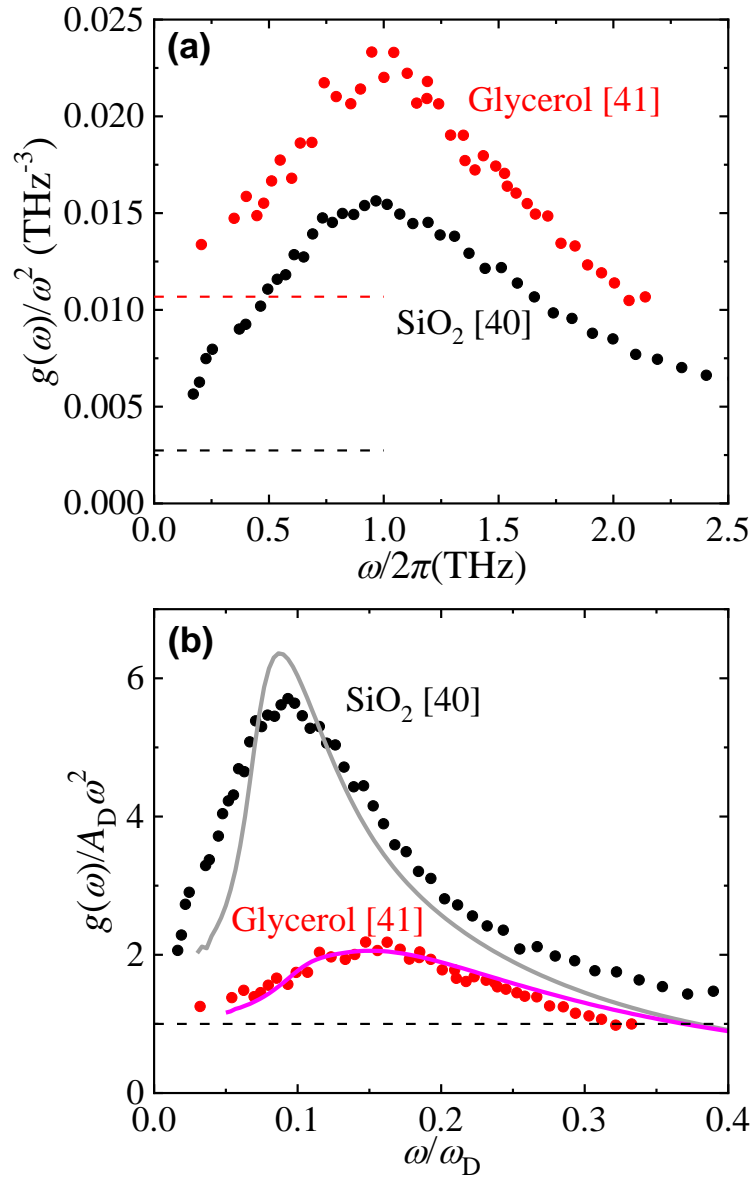


Figure 1 | Boson peak spectra of SiO₂ and glycerol. **a** Boson peaks in the $g(\omega)/\omega^2$ spectrum of SiO₂ and glycerol. The data of SiO₂ and glycerol obtained by inelastic neutron scattering measurements are quoted from the literature^{40,41}, respectively. Black and red dashed lines indicate Debye levels of SiO₂ and glycerol, respectively. **b** Normalised BP plots of SiO₂ and glycerol. The vertical axis was normalised to the Debye level, and the horizontal axis was normalised to the Debye frequency. The grey and pink solid lines show the CPA results for SiO₂ and glycerol, respectively.

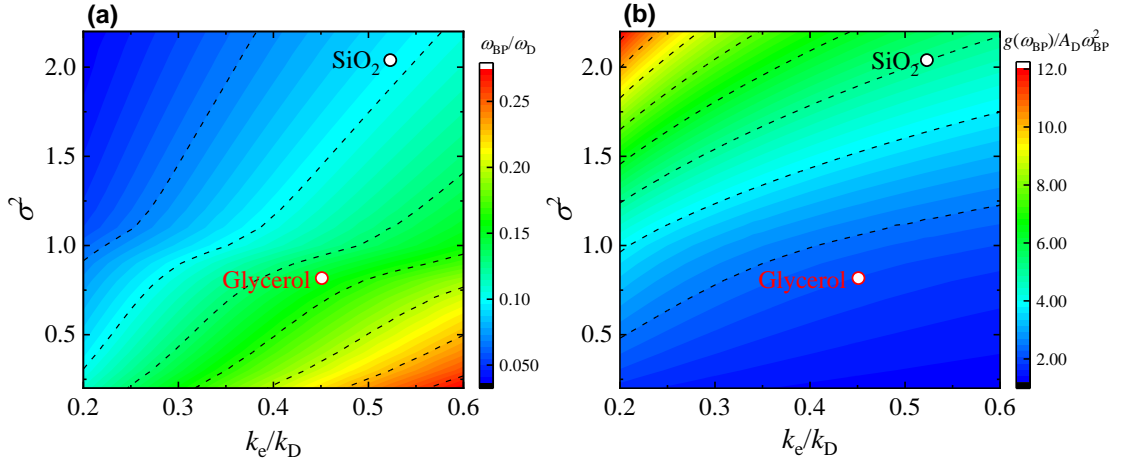


Figure 2 | $k_e - \sigma^2$ dependence of normalised BP frequency and normalised BP intensity. The locations of **a** normalised BP frequency and **b** normalised BP intensity of SiO_2 (black open circles) and glycerol (red open circles) on the $k_e - \sigma^2$ planes obtained by CPA analysis. The input parameters for each glass used for the CPA analysis are summarised in Table S1. Colour maps indicate the $k_e - \sigma^2$ dependence of the normalised BP frequency and normalised BP intensity obtained by CPA analysis for Eq. (2) with $v_L/v_T = 2$, which is a typical ratio for various glasses. The resolutions of k_e and σ^2 are 0.01 and 0.1, respectively. Contours are drawn by dashed lines for the normalised BP frequency every 0.032 and for the normalised BP intensity every 1.30.

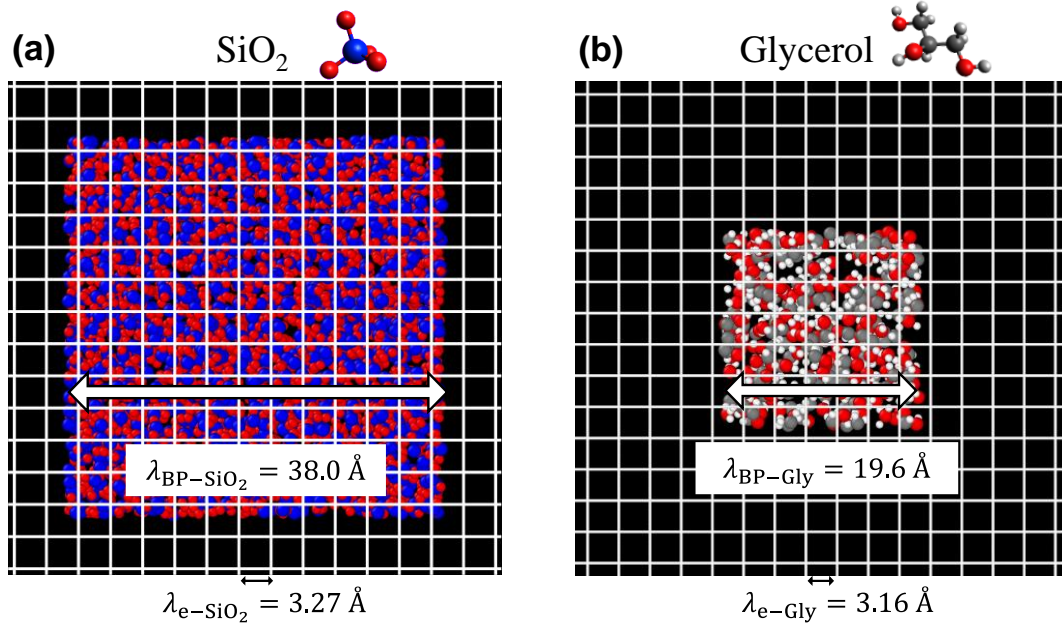


Figure 3 | BP mode wavelength λ_{BP} and minimum possible coarse-graining length λ_e of SiO₂ and glycerol. Glass structures of **a** SiO₂ and **b** glycerol. The dimension of each glass structure indicates the wavelength of each BP mode. The lattice size of the grid lines indicates the minimum possible coarse-graining length λ_e . The visualization of glass structures was carried out through Ovito ⁴².

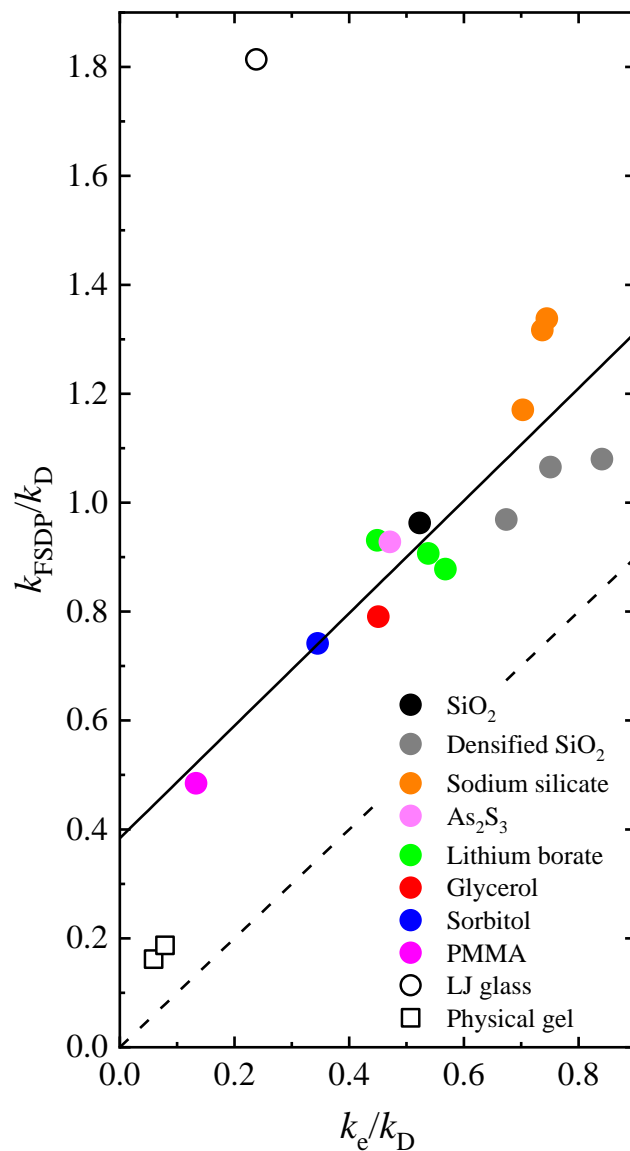


Figure 4 | Relationship between the FSDP wavenumber k_{FSDP} and the maximum possible coarse-graining wavenumber k_e for various glasses. Both k_{FSDP} and k_e were normalised by the Debye wavenumber k_D . The parameters for each glass are summarised in Table S1. The solid line indicates the fitting function obtained by the least-squares method for FSDP glasses, where $k_{\text{FSDP}}/k_D = 1.0 \pm 0.16 k_e/k_D + 0.38 \pm 0.094$, and the correlation coefficient is 0.883. The dashed line indicates a proportional line with slope 1. Open circles and open squares show the results of LJ glass and physical gels, respectively.

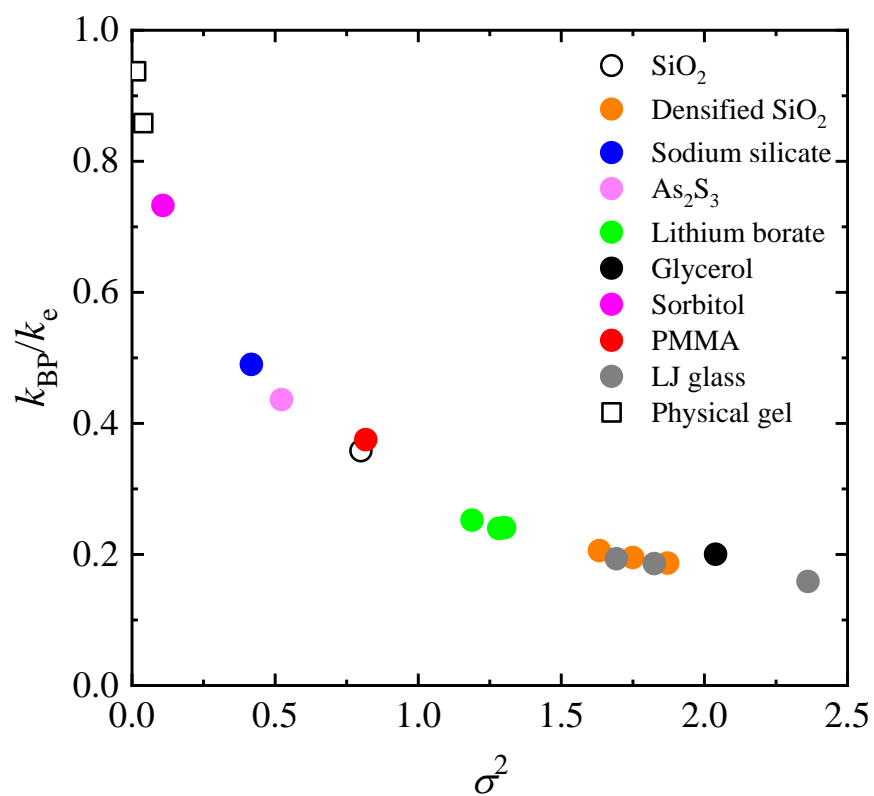


Figure 5 | Relationship between the BP wavenumber k_{BP} and the disorder parameter σ^2 for various glasses. k_{BP} was normalised by the maximum coarse-grained wavenumber k_e . The parameters for each glass are summarised in Supplementary Table S1.

Table 1 | Extracted parameters in CPA analysis of the SiO₂ and glycerol. Normalised maximum possible coarse-graining wavenumber k_e/k_D , minimum possible coarse-graining wavelength λ_e , disorder parameter of spatial distribution of shear modulus σ^2 , geometric mean of spatial distribution of shear modulus G_0 , ratio of k_{BP} to k_e , BP wavelength λ_{BP} , normalised FSDP wavenumber k_{FSDP}/k_D , and Debye wavenumber k_D .

	k_e/k_D	λ_e (Å)	σ^2	G_0 (GPa)	k_{BP}/k_e	λ_{BP} (Å)	k_{FSDP}/k_D	k_D (Å ⁻¹)
SiO ₂	0.523	3.27	2.04	57.2	0.200	38.0	0.96	1.58 ¹
Glycerol	0.451	3.16	0.82	5.43	0.375	19.6	0.79 ²	1.90 ³

¹Reference 31.

²Reference 45.

³Reference 46.

Supplementary Information

Relationship between the boson peak and first sharp diffraction peak in glasses

Dan Kyotani^{1,†}, Soo Han Oh^{1,†}, Suguru Kitani², Yasuhiro Fujii^{3,4}, Hiroyuki Hijiya⁵, Hideyuki Mizuno⁶, Shinji Kohara⁷, Akitoshi Koreeda⁸, Atsunobu Masuno⁹, Hitoshi Kawaji², Seiji Kojima¹, Yohei Yamamoto¹, Tatsuya Mori^{1*}

¹Department of Materials Science, University of Tsukuba, 1-1-1 Tennodai, Tsukuba, Ibaraki 305-8573, Japan

²Materials and Structures Laboratory, Institute of Integrated Research, Institute of Science Tokyo, 4259 Nagatsuta, Midori-ku, Yokohama 226-8501, Japan

³Institute for Open and Transdisciplinary Research Initiatives, Osaka University, 2-1 Yamadaoka, Suita, Osaka 565-0871, Japan

⁴Research Organization of Science and Technology, Ritsumeikan University, 1-1-1 Noji-higashi, Kusatsu, Shiga 525-8577, Japan

⁵Materials Integration Laboratories, AGC Inc., 1-1 Suehiro-cho, Tsurumi-ku, Yokohama 230-0045, Japan

⁶Graduate School of Arts and Sciences, The University of Tokyo, 3-8-1 Komaba, Meguro-ku, Tokyo 153-8902, Japan

⁷Center for Materials Research by Information Integration (CMI2), Research and Services Division of Materials Data and Integrated System (MaDIS), National Institute for Materials Science (NIMS), 1-1 Namiki, Tsukuba, Ibaraki 305-0044, Japan

⁸Department of Physical Sciences, Ritsumeikan University, 1-1-1 Noji-higashi, Kusatsu, Shiga 525-8577, Japan

⁹Graduate School of Engineering, Kyoto University, Kyotodaigaku-Katsura, Nishikyo-ku, Kyoto 615-8520, Japan

*Corresponding author

Email: mori@ims.tsukuba.ac.jp (T. Mori)

†These authors contributed equally to this work.

Content

This file contains Supplementary Figures S1–S7, Supplementary Table S1, and Supplementary References 1–23.

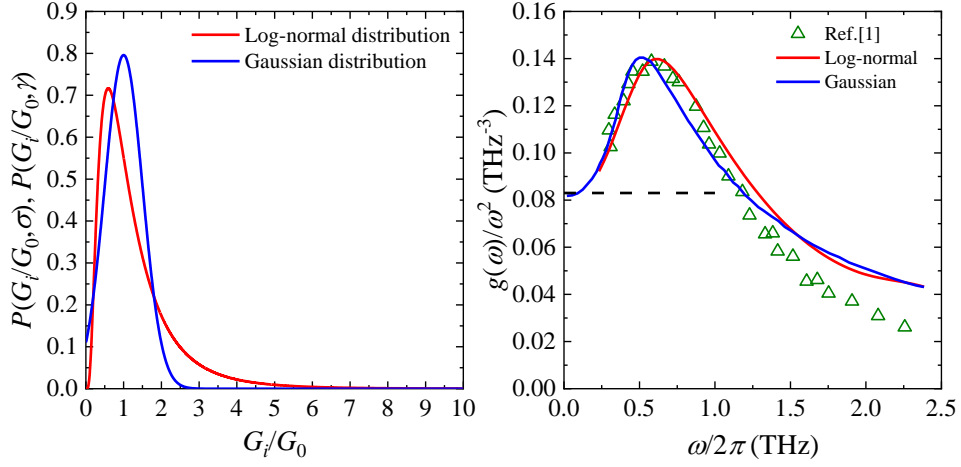


Figure S1. Comparison of BP spectra calculated using log-normal and normal distribution functions. (Left) The log-normal (red line) and normal distribution (blue line) graphs of the probability density function of shear modulus used in HET to reproduce the BP spectrum of As_2S_3 glass. The parameters of the normal distribution function $P(G, \gamma) = \exp(-(G - G_0)^2/\gamma^2)/\sqrt{2\pi\gamma}$, where $\gamma = 0.352 \times v_T^4$ [km^4/s^4] with $v_T = 1.4$ [km/s] and $G_0 = 7.28$ GPa are from a previous study ¹. (Right) BP spectra $g(\omega)/\omega^2$ calculated using log-normal (red line) and normal distribution (blue line) functions for As_2S_3 glass. Black dashed line indicates Debye level of As_2S_3 glass. The spectrum from normal distribution (blue line) and experimental spectrum (green opened triangles) were extracted from a previous study ¹.

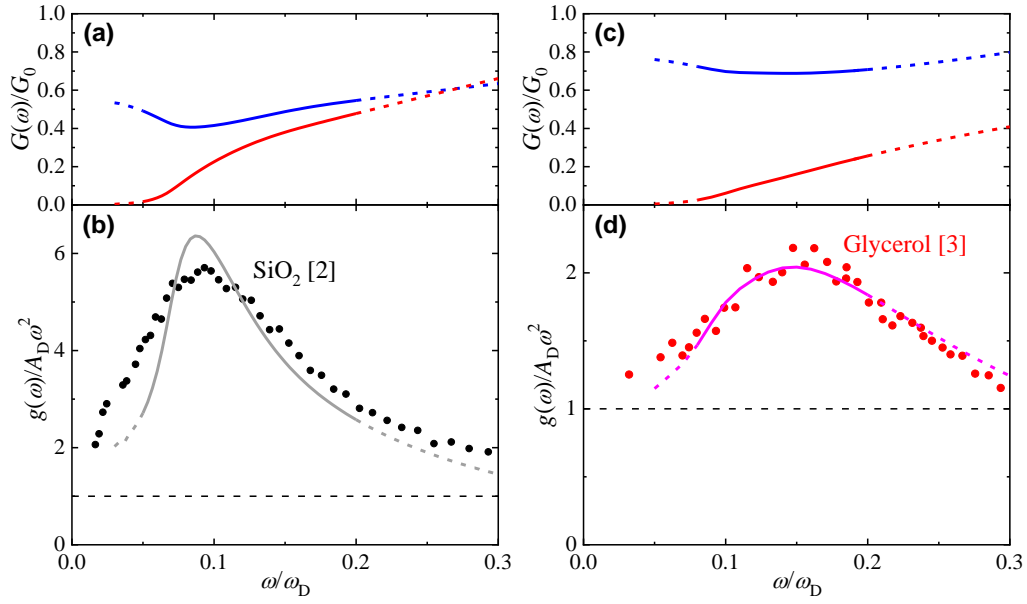


Figure S2. CPA fit results for BP spectra of SiO₂ and glycerol. Real (blue) and imaginary (red) part of $G(\omega)/G_0$ of **a** SiO₂ and **c** glycerol. The solid line part indicates the fitted range, and the rest is indicated by the dashed line. G_0 of SiO₂ and glycerol are 40.1 GPa and 6.4 GPa, respectively. Normalised BP plots of **b** SiO₂ and **d** glycerol. The vertical axis was normalised by Debye level, and the horizontal axis was normalised by Debye frequency. Grey and pink solid lines show the results of CPA analysis for SiO₂ and glycerol, respectively. The filled circles show the experimental data of SiO₂ (black) and glycerol (red), respectively. The data of SiO₂ and glycerol are quoted from previous studies^{2,3}.

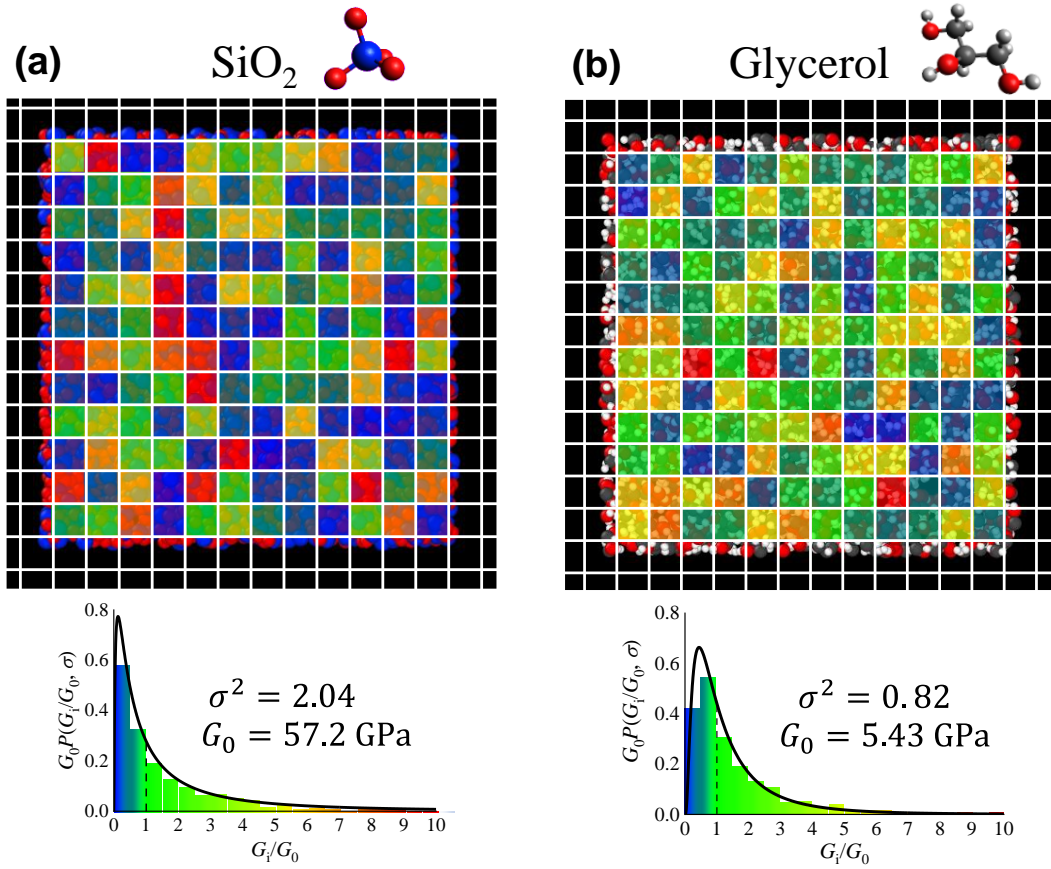


Figure S3. Schematic of the spatial distribution of shear modulus G_i of SiO_2 and glycerol. Colour distributions at the upper part of the figure show the spatial distribution of G_i/G_0 following the log-normal distribution function on **a** SiO_2 and **b** glycerol structures. The lattice size of the grid lines indicates the minimum possible coarse-graining length λ_e . The lower part of the figure shows the log-normal distribution functions of **a** SiO_2 and **b** glycerol obtained by CPA analysis. The colours used in the histogram correspond to the colours of the spatial distribution of G_i/G_0 shown in the upper part of the figure. The parameters of the lattice size λ_e and the log-normal distribution function (G_0 and σ) are summarised in Table 1. The structure of SiO_2 was obtained by reverse Monte Carlo simulation of the structure factors of SiO_2 ⁴. The structure of glycerol was obtained by performing MD simulation of glycerol with the LAMMPS package ⁵ using Chelli's potential ⁶. The visualisation of glass structures was conducted through OVITO ⁷.

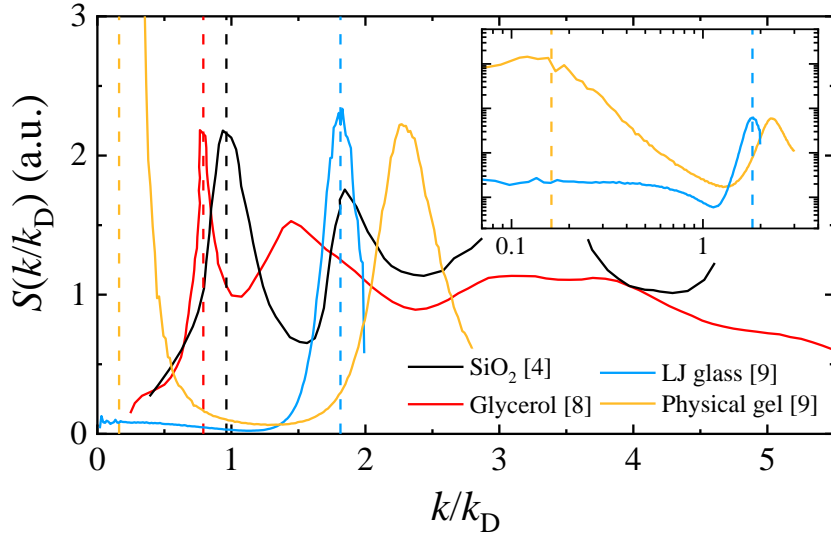


Figure S4. Structural factors of SiO₂, glycerol, LJ glass and physical gel. The horizontal axis of k is normalised by k_D . The FSDPs of silica glass (black line) and glycerol (red line) are located at 0.96 and 0.76, respectively. The inset shows log-log plot of structure factors of LJ glass (cyan line) and physical gel (yellow line). The lowest peaks of LJ glass and physical gel with $\rho = 0.5$ are located at 1.81 and 0.16, respectively. The data of SiO₂ and glycerol were quoted from previous studies ^{4,8}. The data of LJ glass and physical gel were quoted from a previous study ⁹.

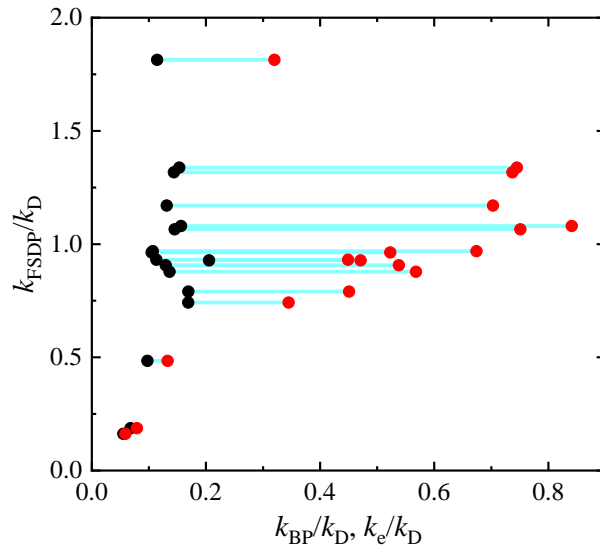


Figure S5. Relationship between the FSDP wavenumber k_{FSDP} and the BP wavenumber k_{BP} for various glasses. k_{FSDP} , k_{BP} and k_{e} were all normalised by the Debye wavenumber k_{D} . $k_{\text{BP}}/k_{\text{D}}$ (black circle) and $k_{\text{e}}/k_{\text{D}}$ (red circle) of the same substance are connected by a solid cyan line for visibility. The parameters for each glass are summarised in Supplementary Table S1.

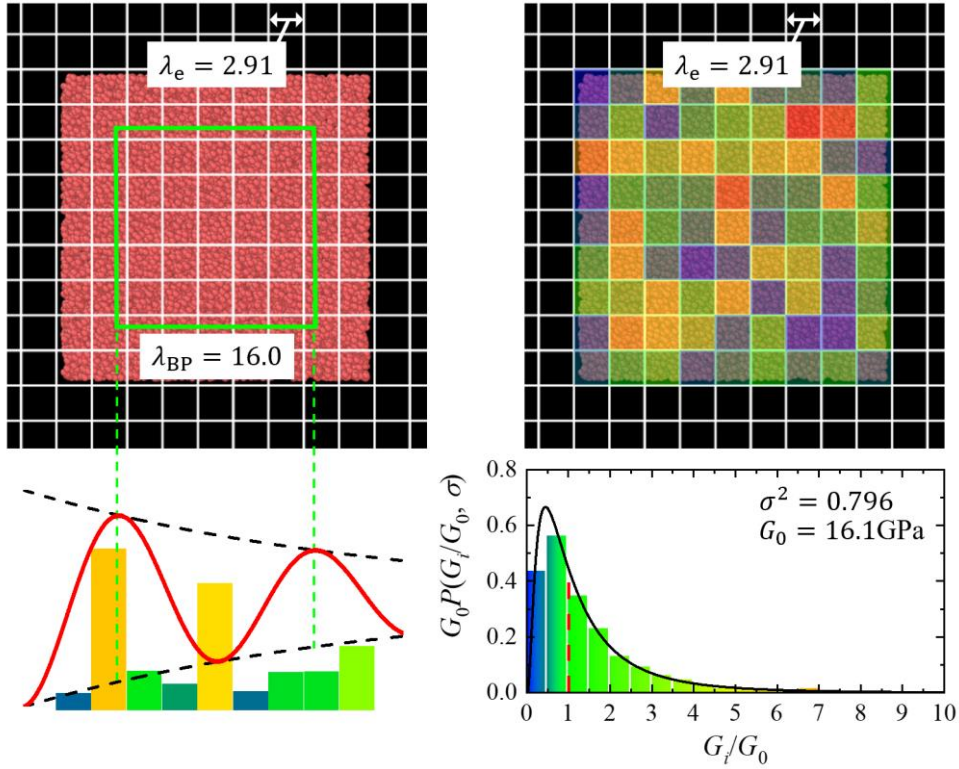


Figure S6. Visualization of results of CPA analysis on LJ glass ($\rho = 1.0$). (Left upper) The lattice size of the grid lines and length of one side of the green square on the LJ glass structure indicate the minimum possible coarse-graining length λ_e and BP wavelength λ_{BP} , respectively. (Left bottom) The red line represents a sound wave with a wavelength of λ_{BP} that is attenuated by a random shear modulus distribution. (Right upper) The colour distribution shows the spatial distribution of G_i/G_0 following the log-normal distribution function on the LJ glass structure. The lattice size of the grid lines indicates the minimum possible coarse-graining length λ_e . (Right bottom) The log-normal distribution functions of LJ glass obtained by CPA analysis. The colours used in the histogram correspond to the colours of the spatial distribution of G_i/G_0 shown in the upper part of the figure. The parameters of the lattice size λ_e and the log-normal distribution function (G_0 and σ) are summarised in Table 1.

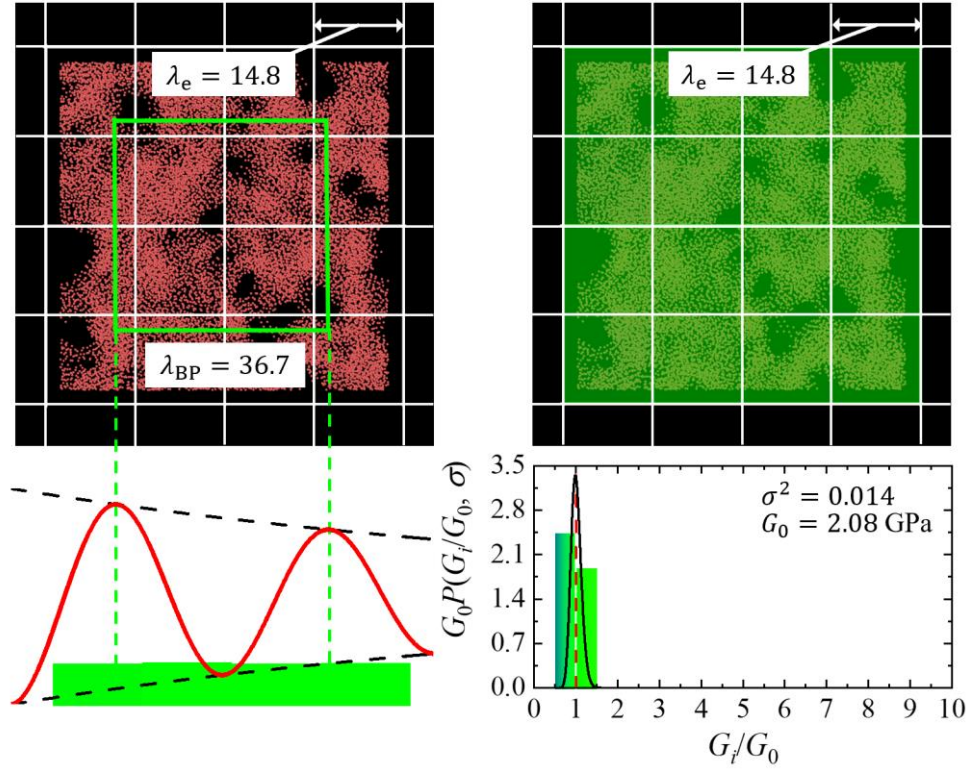


Figure S7. Visualization of results of CPA analysis on physical gel ($\rho = 0.5$). (Left upper) The lattice size of the grid lines and length of one side of the green square on the physical gel structure indicate the minimum possible coarse-graining length λ_e and BP wavelength λ_{BP} , respectively. (Left bottom) The red line represents a sound wave with a wavelength of λ_{BP} that is attenuated by a random shear modulus distribution. (Right upper) Colour distribution shows the spatial distribution of G_i/G_0 following the log-normal distribution function on physical gel structure. The lattice size of the grid lines indicates the minimum possible coarse-graining length λ_e . (Right bottom) The log-normal distribution functions of LJ glass obtained by CPA analysis. The colours used in the histogram correspond to the colours of the spatial distribution of G_i/G_0 shown in the upper part of the figure. The parameters of the lattice size λ_e and the log-normal distribution function (G_0 and σ) are summarised in Table 1.

Table S1. Input and extracted parameters in the CPA analysis. Mass density ρ , transverse v_T and longitudinal v_L sound velocities, normalised maximum possible coarse-graining wavenumber k_e/k_D , minimum possible coarse-graining wavelength λ_e , disorder parameter of spatial distribution of shear modulus σ^2 , geometric mean of spatial distribution of shear modulus G_0 , ratio of k_{BP} to k_e , BP wavelength λ_{BP} , normalised FSDP wavenumber k_{FSDP}/k_D , and Debye wavenumber k_D . Sodium silicate glass, lithium borate glass and polymethyl methacrylate are abbreviated as NS, LiB and PMMA, respectively. $g(\omega)$ of densified SiO₂, NS, and LiB were determined from the specific heat data by maximum entropy method analysis¹⁰.

	ρ (g/cm ⁻³)	v_T (m/s)	v_L (m/s)	k_e/k_D	λ_e (Å)	σ^2	G_0 (GPa)	k_{BP}/k_e	λ_{BP} (Å)	k_{FSDP}/k_D	k_D (Å ⁻¹)
SiO ₂ [4]	2.21 [4]	3746 [4]	6058 [4]	0.523	3.27	2.04	57.2	0.200	38.0	0.96 [4]	1.58
Densified SiO ₂ (7.7 GPa, RT)	2.24 [4]	3744 [11]	5902 [11]	0.674	2.53	2.36	65.4	0.159	37.1	0.97 [4]	1.59
Densified SiO ₂ (7.7 GPa, 600 °C)	2.66 [4]	4101 [11]	6694 [11]	0.751	2.14	1.69	73.0	0.193	25.8	1.07 [4]	1.68
Densified SiO ₂ (7.7 GPa, 800 °C)	2.68 [4]	4180 [11]	6921 [11]	0.841	1.91	1.83	78.9	0.186	23.9	1.08 [4]	1.68
NS2	2.49 [12]	3070 [12]	5360 [12]	0.745	2.22	1.63	37.7	0.206	25.0	1.34 [13]	1.64
NS3	2.43 [12]	3159 [12]	5347 [12]	0.737	2.26	1.75	39.5	0.195	26.9	1.32 [13]	1.63
NS4	2.38 [12]	3251 [12]	5382 [12]	0.703	2.38	1.87	43.0	0.187	29.6	1.17 [13]	1.61
As ₂ S ₃ [14]	3.14 [15]	1418 [15]	2625 [15]	0.471	4.36	0.52	7.28	0.436	23.3	0.93 [16]	1.32
LiB8	1.95 [17]	2489	4491	0.449	3.50	1.19	16.5	0.252	32.3	0.93 [18]	1.72
LiB14	2.05 [17]	2915	5310	0.538	2.87	1.30	24.4	0.241	27.7	0.91 [18]	1.75
LiB22	2.16 [17]	3388	6098	0.568	2.65	1.28	34.7	0.240	25.7	0.88 [18]	1.79
Glycerol [2]	1.26 [19]	1871 [19]	3614 [19]	0.451	3.16	0.82	5.43	0.375	19.6	0.79 [7]	1.90
Sorbitol [20]	1.47 [21]	2107 [20]	4081 [20]	0.345	4.01	0.42	7.29	0.490	19.0	0.74 [20]	1.96
PMMA [21]	1.19	1420 [23]	2780 [23]	0.133	10.8	0.11	2.47	0.732	34.3	0.48 [23]	1.88
LJ glass [9]	1.0 [9]	3683 [9]	9113 [9]	0.238	2.91	0.80	16.1	0.364	16.0	1.81 [9]	3.90
Physical gel ($\rho=0.7$) [9]	0.7 [9]	2524 [9]	4424 [9]	0.079	9.89	0.04	4.52	0.858	26.8	0.19 [9]	3.46
Physical gel ($\rho=0.5$) [9]	0.5 [9]	2034 [9]	3516 [9]	0.059	14.8	0.01	2.08	0.937	36.7	0.16 [9]	3.09

Supplementary References

- [1] Schmid, B. & Schirmacher, W. Raman Scattering and the Low-Frequency Vibrational Spectrum of Glasses. *Phys. Rev. Lett.* **100**, 137402 (2008).
- [1] Wischniewski, A., Buchenau, U., Dianoux, A. J., Kamitakahara, W. A. & Zarestky, J. L. Sound-wave scattering in silica. *Phys. Rev. B* **57**, 2663 (1998).
- [2] Wuttke, J., Petry, W., Coddens, G., & Fujara, F. Fast dynamics of glass-forming glycerol. *Phys. Rev. E* **52**, 4026 (1995).
- [3] Onodera, Y. *et al.* Structure and properties of densified silica glass: characterizing the order within disorder. *NPG Asia Mater.* **12**, 85 (2020).
- [4] Plimpton, S. Fast parallel algorithms for short-range molecular dynamics. *J. Comput. Phys.* **117**, 1 (1995).
- [5] Chelli, R. *et al.* Glycerol condensed phases Part I. A molecular dynamics study. *Phys. Chem. Chem. Phys.* **1**, 871–877 (1999).
- [6] Stukowski, A. Visualization and analysis of atomistic simulation data with OVITO—the open visualization tool. *Modeling Simul. Mater. Sci. Eng.* **18**, 015012 (2010).
- [7] Champeney, D.C., Joarder, R. N., & Dore, J. C. Structural studies of liquid D-glycerol by neutron diffraction. *Mol. Phys.* **58**, 337–347 (1986).
- [8] Mizuno, H., Hachiya, M. & Ikeda, A. Structural, mechanical, and vibrational properties of particulate physical gels. *J. Chem. Phys.* **155**, 234502 (2021).
- [9] Mori, T. *et al.* Detection of boson peak and fractal dynamics of disordered systems using terahertz spectroscopy. *Phys. Rev. E* **102**, 022502 (2020).
- [11] Masuno, A., Nishiyama, N., Sato, F., Kitamura, N., Taniguchi, T. & Inoue, H. Higher refractive index and lower wavelength dispersion of SiO₂ glass by structural ordering evolution via densification at a higher temperature. *RSC Adv.* **6**, 19144 (2016).
- [12] Bansal, N. P. & Doremus, R. H. *Handbook of glass properties* (Academic Press, Inc., 1986).
- [13] Waseda, Y. & Suito, H. The structure of the molten FeO-SiO₂ system. *Trans. Iron Steel Inst. Jpn.* **17**, 82 (1977).
- [14] Malinovsky, V. K., Novikov, V. N., Parshin, P. P., Sokolov, A. P. & Zemlyanov, M. G. Universal form of the low-energy (2 to 10 meV) vibrational spectrum of glasses. *Europhys. Lett.* **11**, 43 (1990).
- [15] Sawamura, S. & Wondraczek, L. Scratch hardness of glass. *Phys. Rev. Mater.* **2**, 092601(R) (2018).
- [16] N'Dri, K., Houphouet-Boigny, D. & Jumas, J. C. Study of first sharp diffraction peak in As₂S₃ glasses by X-ray powder diffraction method. *J. Non-Oxide Glass* **3**, 29 (2012).
- [17] Kodama, M., Matsushita, T. & Kojima, S. Velocity of sound and elastic properties of Li₂O-

- B₂O₃ glasses. *Jpn. J. Appl. Phys.* **34**, 2570 (1995).
- [18] Swenson, J., Börjesson, L. & Howells, W. S. Structure of borate glasses from neutron-diffraction experiments. *Phys. Rev. B* **52**, 9310 (1995).
- [19] Scarponi, F., Comez, L., Fioretto, D. & Palmieri, L. Brillouin light scattering from transverse and longitudinal acoustic waves in glycerol. *Phys. Rev. B* **70**, 054203 (2004).
- [20] Ruta, B., Ph.D. dissertation, Université Joseph Fourier, Grenoble, (2010).
- [21] Naoki, M., Ujita, K. & Kashima, S. Pressure-volume-temperature relations and configurational energy of liquid, crystal, and glasses of D-sorbitol. *J. Phys. Chem.* **97**, 12356–12362 (1993).
- [22] Duval, E. *et al.* Inelastic light, neutron, and X-ray scattering related to the heterogeneous elasticity of glasses. *J. Non-Cryst. Solids* **105**, 307–310 (2002).
- [23] Sokolov A. P., Kisliuk, A., Soltwisch, M. & Quitmann, D. Medium-range order in glasses: Comparison of Raman and diffraction measurements. *Phys. Rev. Lett.* **69**, 1540 (1992).